ALGEBRAIC FLUX CORRECTION FOR EQUI-DIMENSIONAL TRANSPORT PROBLEMS IN POROUS FRACTURED MEDIA

MARIA GIUSEPPINA CHIARA NESTOLA[1], MARCO FAVINO[2]

[1] Universitá della Svizzera italiana
6900 Lugano Switzerland
nestom@usi.ch

[2] Universitá della Svizzera italiana
6900 Lugano Switzerland
marco.favino@usi.ch

Key words: Fractured porous media, Coupled transport problems, Equi-dimensional models, Adaptive mesh refinement, Algebraic flux correction.

Abstract. We present a simple finite element framework which enables numerical simulations of transport problems in fractured porous media based on equi-dimensional models, i.e., models where fractures are considered heterogeneities of the same geometrical dimension as the embedding background. The two main ingredients of the proposed framework are an adaptive mesh refinement strategy, and an algebraic flux correction stabilization.

The proposed finite-element method for equi-dimensional models is inherently simple and can be easily implemented in any common simulation software, as it does not require the complicated management of different meshes and discretizations, which are necessary for numerical simulations based on hybrid-dimensional models, i.e., models where fractures are considered as heterogeneities of a lower geometrical dimension than the embedding background. Actually, our equi-dimensional approach provides a strategy to validate hybrid-dimensional models. Our adaptive approach is inherently conservative and naturally reduces the discretization error which, for problems with heterogeneities, is concentrated at the interfaces.

1 Introduction

Numerical simulations of transport problems in fractured porous media are of fundamental importance for numerous applications, such as geothermal energy production, hydrocarbon exploration, nuclear waste disposal, and CO_2 storage. Fractures in a porous medium are heterogeneities in an embedding background that can be arranged in complex networks. Fractures are characterized by one dimension, the *aperture*, which is orders-of-magnitude smaller than the characteristic size of the background, and by material properties which also differ by orders-of-magnitude from the ones of the background.

Numerical simulations of fractured media are particularly challenging for the following reasons. First, the mesh generation of full *equi-dimensional* models, i.e., models which represent

the fractures as heterogeneity of the same geometric dimension as the background, is considered practically unfeasible for realistic fracture networks [1, 2, 3, 4]. Second, analytical solutions of problems with heterogeneous material properties and/or mixed boundary conditions are generally characterized by a singular behaviour, i.e., there exist so-called singular points where the solution and/or its derivative are not bounded [5]. In the vicinity of singular points, standard discretization methods are characterized by a low accuracy with respect to the order of the method [6]. Third, standard discretization methods for the numerical simulation of pure advection problems, which describe the transport of a concentration in a fractured porous medium, usually do not satisfy the discrete maximum (DMP) and the discrete monotonicity principles [7]. A violation of the DMP manifests itself in unphysical oscillations and negative values of the solution, which are not acceptable for positive quantities, such as concentrations. Stabilization techniques, which consist in or are equivalent to the introduction of a mesh dependent diffusion term [8, 9, 7], are at best first-order accurate due to the Godunov barrier [10] and may produce overly diffusive numerical results.

In this work, we propose a simple finite element (FE) approach based on the adaptive mesh refinement (AMR) technique and algebraic flux correction (AFC) stabilization for numerical simulations of transport problems in porous fractured media based on an equi-dimensional model. We employ an AMR strategy similar to the one proposed in [11, 12] to adapt an initial coarse mesh to any fracture distribution. As these meshes do not resolve the interfaces, they will be referred to as *unresolved*. We point out that this approach has been already employed to solve for single-phase flow problem in porous fractured media [12] and validated in [13].

The paper is organized as follows. In Section 2, we briefly describe the AMR strategy for the mesh generation. In Section 3, we present the differential equations of the transport problem, introduce their FE formulation and present the AFC strategy. In Section 4, benchmark problems are used to evaluate the performance of our approach in terms of approximation properties. Finally, in Section 5, we draw some concluding remarks.

2 Geometry of fractured media

For the generation of meshes for heterogeneous fractured media, we employ the adaptive mesh refinement (AMR) strategy proposed in [11]. The fundamental concept in their approach involves initiating with a coarse (uniform) initial mesh. Then, given a distribution of fractures, the algorithm refines the elements that have non-empty overlap with at least one of them, at each step of the AMR algortithm. In our approach, we focus on refining the elements that have a non-empty intersection with the boundary of a fracture.

Through the iterative application of this AMR procedure, we generate a hierarchy of meshes that progressively refine toward the interfaces between fractures and the embedding background and in the neighbourhood of singular points. The AMR strategy automates the creation of meshes for any heterogeneity distribution without requiring human intervention. As the resulting meshes do not resolve the interfaces between the background and the fracture domains, we refer to them as *unresolved* meshes.

We start from a mesh $\mathcal{U}^{\mathrm{be}}$ that is uniform and regular. The integer be refers to the number

of elements of elements along the x_1 axis. The number of elements along the other axis are chosen proportionally to the size of the domain Ω. We denote the mesh obtained from amr steps of refinement process by $\mathcal{U}_{\text{amr}}^{\text{be}}$. By increasing values of amr, we can generate meshes, which become progressively finer close to the interface between fractures and matrix, where the discretization error is usually larger.

A fundamental parameter for unresolved meshes is the accuracy with which they approximate the interface. We denote this parameters by w defined as

$$w = \frac{\delta}{\frac{L_1}{\text{be } 2^{\text{amr}}}}. \tag{1}$$

We observe that w is the ratio between the fracture aperture δ and the dimension of the smallest elements generated by the AMR strategy.

3 Transport problem

The discretization proposed in this work is based on low-order FE and meshes which are automatically adapted to the geometrical features of domain.

Meshes are a decomposition of Ω into elements, which are axis-aligned squares in two-dimensional settings, or cubes, in three-dimensional settings. As they are supposed to be created from an adaptive process, they may present hanging nodes, i.e., there could be a vertex of an element which may belong to the edge or to the face of another element. Non-hanging nodes are instead said to be regular.

We consider low-order nodal conforming FE discretizations and we associate a Lagrangian basis function to each regular node. Hanging nodes do not have an associated basis function in case of conforming discretizations.

We denote the index set of regular nodes by J^R, and define $J^D \subset J^R$ as the index set of the nodes which belongs to the Dirichlet boundary Γ_D, i.e. $J^D = \{i \,:\, \mathbf{x}_i \in \Gamma_D\}$. We let S^h denote the nodal interpolation space over $\mathcal{T}$ defined as

$$S^h = \{v \in C^0(\Omega) \,:\, v|_E \in \mathbb{Q}_1\},$$

where $\mathbb{Q}_1$ is the space of multi-linear functions on E. We call N_i the Lagrangian basis function associated with the vertex V_i. Observe that the space $S^h = \text{span}\{N_i\}_{i \in J^R}$.

We also define

$$U^h = \{v^h \in S^h \text{ such that } v_h(\mathbf{x}_i) = g(\mathbf{x}_i) \, \forall i \in J^D\}$$

and

$$V^h = \{v^h \in S^h \text{ such that } v_h(\mathbf{x}_i) = 0 \, \forall i \in J^D\}.$$

Transport problem

We let $\mathscr{I} = (0, T_{\text{fin}}]$ denote a time interval, $\Gamma_{in} := \{\mathbf{x} \in \partial\Omega \,:\, \underline{u} \cdot \underline{n} < 0\}$ denote the inflow boundary, and $\Gamma_{out} := \{\mathbf{x} \in \partial\Omega \,:\, \underline{u} \cdot \underline{n} \geq 0\}$ denote the outflow boundary. Moreover, we

also assume $\Gamma_{in} = \Gamma_D$. The strong formulation of the equi-dimensional transport problem for a concentration $c = c(\mathbf{x}, t)$ reads

$$
\begin{cases}
\phi \dfrac{\partial c}{\partial t} + \nabla \cdot (\underline{u}\, c) & = & 0 & \text{in } \Omega \times \mathscr{I} \\
c(\,\cdot\,, 0) & = & c_0 & \text{in } \Omega \\
c & = & g & \text{on } \Gamma_{in} \times \mathscr{I}
\end{cases}
\tag{2}
$$

where c_0 is the initial condition, ϕ is the porosity (i.e. a material parameter which may attain different values in the background matrix and in the fracture network), and g is the Dirichlet boundary condition. The transport problem is coupled to the flow problem through the velocity field $\underline{u} = -k\nabla P$, where k represents the permeability and P is the solution field of the flow problem. The flow problem is solved by means of the approach presented in [12] and validated in [13]. The finite-element discretization of the transport problem (2) reads as

For all $t \in \mathscr{I}$, find $c_h(\,\cdot\,, t) \in U_h$ such that $c(\,\cdot\,, 0) = c_0$, and

$$
m\left(\frac{\partial c_h}{\partial t}, q_h\right) = a(c_h, q_h) \quad \forall q_h \in V_h.
\tag{3}
$$

where we have used the following discrete bi-linear forms:

$$
\begin{aligned}
m\left(\frac{\partial c_h}{\partial t}, q_h\right) & = & \int_\Omega \phi\, \frac{\partial c_h}{\partial t}\, q_h\, \mathrm{d}V, \\
a(c_h, q_h) & = & \int_\Omega c_h\, \underline{u} \cdot \nabla q_h\, \mathrm{d}V - \int_{\Gamma_{out}} c_h\, q_h\, \underline{u} \cdot \underline{n}\, \mathrm{d}A,
\end{aligned}
$$

and $c_h = c_h(\,\cdot\,, t) \in U^h$ is the approximation of the concentration c at time t.

Problem (3) admits the following algebraic representation

$$
\mathbf{M}\frac{\mathrm{d}\mathbf{c}}{\mathrm{d}t} = \mathbf{A}\mathbf{c},
\tag{4}
$$

where the matrices $\mathbf{M}$ and $\mathbf{A}$ are the scaled mass matrix and the discrete advection operator, respectively, and $\mathbf{c}$ is a the time dependent array having as components the unknown coefficients c_j with respect to the basis Nj.

3.1 Discrete maximum principle for the transport problem

A classic theorem that provides sufficient conditions to ensure the maximum principle and positivity preservation for the semi-discrete transport problem (4) is the following [7]:

Theorem 1 *Suppose that:*

- $[\mathbf{M}]_{ii} > 0$, *and* $[\mathbf{M}]_{ij} = 0 \,\forall i \neq j$

- $[\mathbf{A}]_{ij} \geq 0 \,\forall i \neq j$.

Then the following a-priori estimates hold for the coefficient c_i:

1a The semi-Discrete Maximum Principle (DMP) is satisfied:

$$\sum_j [\mathbf{A}]_{ij} = 0, \quad and \quad c_i \geq c_j, \quad \forall j \neq i \quad \implies \quad \frac{dc_i}{dt} \leq 0.$$

1b The positivity preservation is satisfied:

$$c_j(0) \geq 0, \forall j \quad \implies \quad c_i(t) \geq 0, \forall t > 0.$$

Continuous FE discretizations applied to transport problems are characterized by under-shoots and overshoots of the numerical solution as the matrices arising are not M-matrices [14]. Several *stabilization* strategies have been proposed to make $\mathbf{M}$ and $\mathbf{A}$ consistent with the hypothesis of theorem 1. In the following, we refer to the AFC predictor-corrector strategy proposed by [7]. The basic idea of this method is to employ an algebraic diffusion operator that allows ensuring the DMP and preserve of positivity of the solution.

The first step of the AFC scheme is to introduce artificial diffusion into the high-order scheme to develop a positivity-preserving scheme. To this aim, a lower order linear transport operator is designed to satisfy the hypotheses of Theorem 1. In particular, one needs to 1) approximate the consistent mass matrix $\mathbf{M}$ by its lumped counterpart $\mathbf{M}_L$ and 2) eliminate the negative off-diagonal entries of the transport operator $\mathbf{A}$ by adding a discrete diffusion operator $\mathbf{S}^A$ such that:

- $[\mathbf{S}^A]_{ij} = \max(-[\mathbf{A}]_{ij}, 0, -[\mathbf{A}]_{ji})$ for $i \neq j$,

- $[\mathbf{S}^A]_{ii} = -\sum_{j \neq i}[\mathbf{S}^A]_{ij}$.

and replacing $\mathbf{A}$ with $\tilde{\mathbf{A}} = \mathbf{A} + \mathbf{S}^A$.

In the process of AFC, the discrete problem (4) is split into a *good* diffusive part of the form

$$\mathbf{T}\,\mathbf{c}^{n+1} = \mathbf{M}_L \mathbf{c}^n,$$

with $\mathbf{T} = \mathbf{M}_L - \Delta t\,\tilde{\mathbf{A}}$ and a *bad* anti-diffusive part given by

$$\mathbf{f} = (\mathbf{M}_L - \mathbf{M})\mathbf{c}^{n+1} - \Delta t\,\mathbf{S}^A \mathbf{c}^{n+1} - (\mathbf{M}_L - \mathbf{M})\mathbf{c}^n.$$

The bad anti-diffusive term admits the decomposition $[\,\mathbf{f}\,]_i = \sum_{j \neq i}[\mathbf{F}]_{ij}$ where the components of the sum represent a numerical flux which attain a local conservation property, i.e. $[\mathbf{F}]_{ij} + [\mathbf{F}]_{ji} = 0$.

The *good* diffusive counterpart is positivity-preserving but overly diffusive due to its linearity. Indeed, due to Godunov's theorem [15] the accuracy of the stabilized FE method decreases to first order. A high-resolution scheme can be reconstructed by locally adding an anti-diffusive correction.

By following the approach proposed in [7], we disregard the antidiffusive term $\mathbf{f}$ and solve the linear system

$$\mathbf{T}\,\mathbf{c}_L^{n+1} = \mathbf{M}_L \mathbf{c}^n.$$

Then, we add the anti-diffusive correction term $[\tilde{\mathbf{f}}]_i = \sum_{j \neq i}[\mathbf{F}]_{ij}[\alpha]_{ij}$ to recover the accuracy of the original high-order discretization as follows

$$\mathbf{M}_L\,\mathbf{c}^{n+1} = \mathbf{M}_L \mathbf{c}_L^{n+1} + \Delta t\,\tilde{\mathbf{f}},$$

where $0 \leq \alpha \leq 1$ is solution-dependent correction factor computed to restrict the amount of anti-diffusion at every regular node [7]. We point out that if all the factors $[\alpha]_{ij}$ are equal to 1 the original high-order Galerkin discretization is recovered, while the lower order discretization is attained for $[\alpha]_{ij} = 0$.

4 Numerical examples

In the following, we validate our approach on two benchmark problems proposed in literature: *Regular Fracture Network* [16, 17], and *Small Features* [13]. The software used to solve the numerical examples is `Parrot2` (`https://github.com/favinom/parrot2`), an application implemented in the FE framework `MOOSE` (`https://mooseframework.inl.gov`). `Parrot2` allows for the simulation of several problems in heterogeneous materials, such as flow, transport, Biot's equations in the space-time and space-frequency domains [18, 19, 11].

4.1 Regular fracture network

The domain Ω of this benchmark example consists of a unit square, i.e., $L_1 = L_2 = 1$ [m], and contains six axis-aligned fractures of aperture $\delta = 10^{-4}$ [m] (see Figure 1a). The material properties and boundary conditions are the ones employed in [16] and [17]. In [17], a further approach based on a hybrid-dimensional formulation for transport problems and an embedded FE method has been presented.

In Figure 1b, we report an example of a initial background mesh, while in Figures 1c and 1d, we report the first two adaptive steps for the generation of unresolved meshes.

For the transport problem Γ_{in} coincide with the left side of Ω. The Dirichlet boundary condition at the inflow is set as $g = 1.0$ [m^{-3}]. We refer to [16, 13] for more details. We set $T_{\text{fin}} = 0.50$ [s] and $\Delta t = 0.025$ [s] and evaluate the concentration profile along the segments CC$'$ ($x_2 = 0.5$) and DD$'$ ($x_2 = 0.75$) at $t = 0.01$ [s], $t = 0.1$ [s], and $t = 0.5$ [s]. We observe that the segment CC$'$ is located along the center of a fracture, while the segment DD$'$ is located in the background and crosses three fractures. We consider the solution obtained on the mesh $\mathcal{U}_7^{1280}$ as the reference solution.

In Figure 2, we report the distribution of the concentration at the three considered times. The concentrations are positive and are significantly different from zero in the horizontal fractures, as the flow is along the horizontal direction.

We analyse the effects of amr and be on the concentration profiles in Figure 3. In Figures 3a, 3c, and 3e, we study the effect of amr by comparing concentration profiles with the

(a) Ω (b) $\mathcal{U}_0^{32}$

(c) $\mathcal{U}_1^{32}$ (d) $\mathcal{U}_2^{32}$
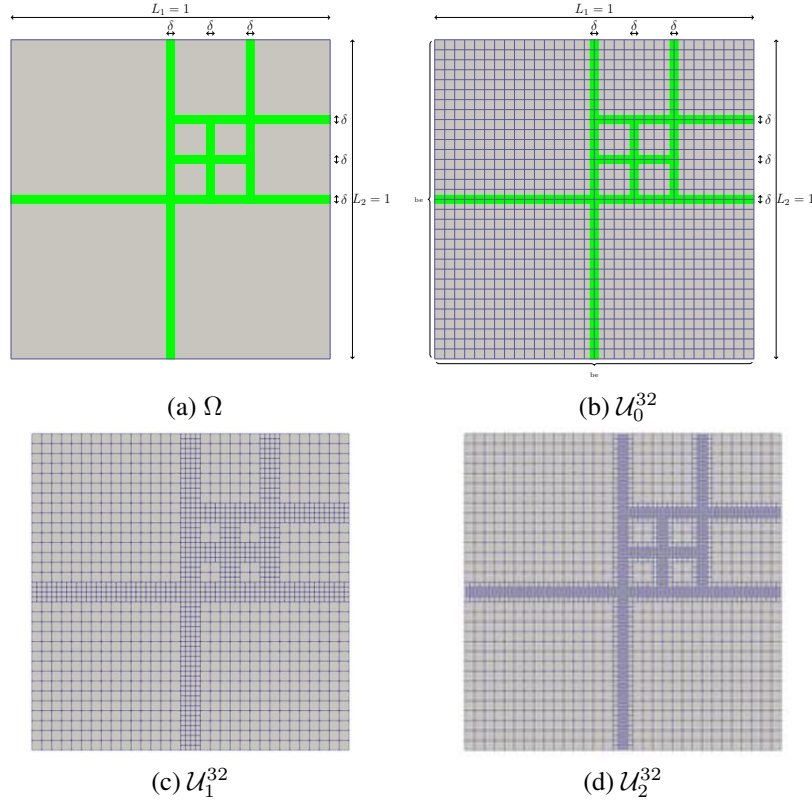
Figure 1: Three steps of AMR procedure to create an *unresolved mesh* $\mathcal{U}_{\mathrm{amr}}^{\mathrm{be}}$ for the regular fracture network example.

same be. We observe that amr plays a minor role on the concentration profiles, as the numerical results obtained with $\mathcal{U}_9^{80}$, $\mathcal{U}_{10}^{80}$, and $\mathcal{U}_{11}^{80}$ are superimposed. The same holds for the results obtained with $\mathcal{U}_9^{160}$ and $\mathcal{U}_{10}^{160}$. This behavior can be observed for both segments CC$'$ and DD$'$, although the differences are more visible along DD$'$, which is mainly located along the background.
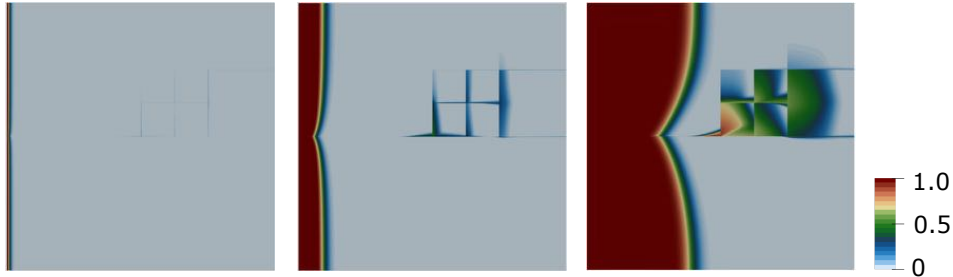
Figure 2: Concentration distribution at time $t_1 = 0.01\,[\mathrm{s}]$, $t_2 = 0.10\,[\mathrm{s}]$, and $t = T_{\mathrm{fin}} = 0.50\,[\mathrm{s}]$ computed with the mesh $\mathcal{U}_7^{1280}$.

These observations are confirmed from the plots reported in Figures 3b, 3d, and 3f, where we study the effect of be by comparing numerical results with the same w. Numerical results show that a fine background mesh is necessary to obtain the steep concentration profile.

These differences are explained mostly by the algebraic diffusion stabilization that ensures the DMP. The algebraic diffusion stabilization is proportional to the local mesh size, i.e., larger elements are characterized by a larger diffusion. Hence, numerical solutions on quite coarse background meshes are overly diffusive, although they ensure the positivity of the concentrations.

(a) t=0.01 s   (b) t=0.01 s

(c) t=0.1 s   (d) t=0.1 s

(e) t=0.5 s   (f) t=0.5 s
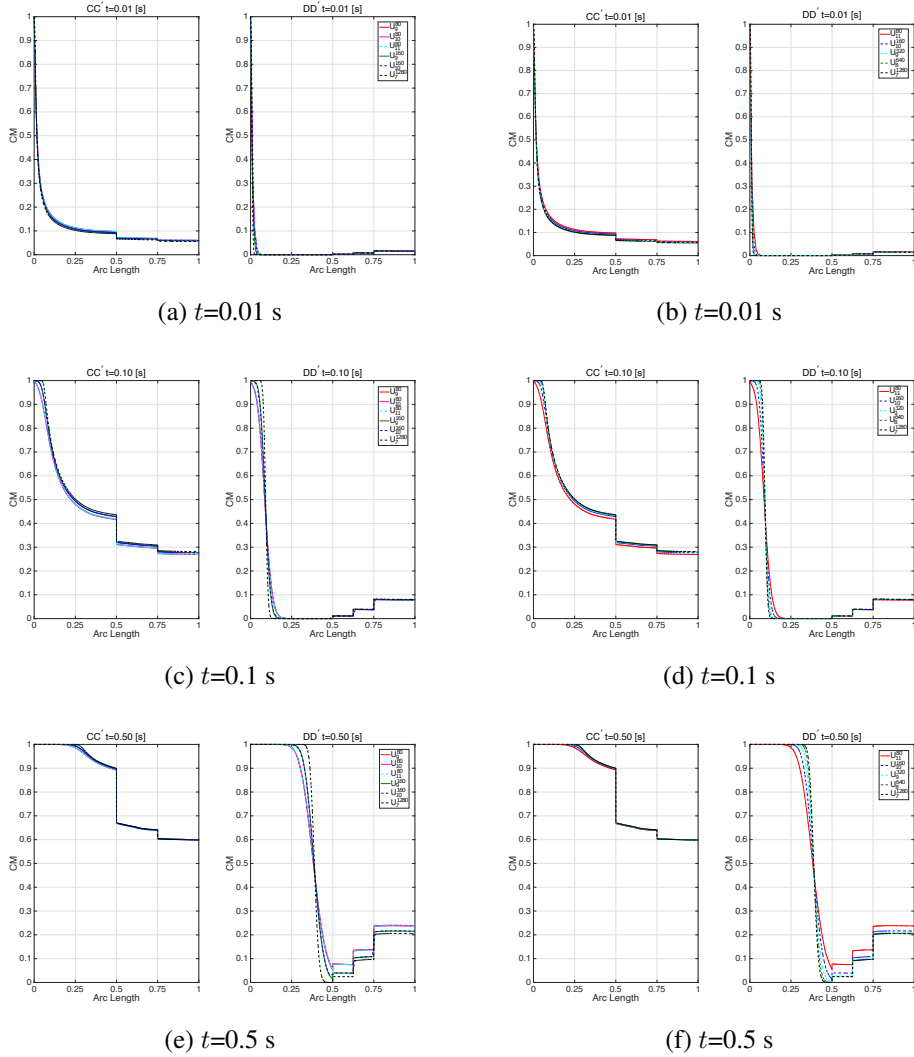
Figure 3: Concentration profiles along the two segments CC' and DD' on unresolved meshes. In the left column (Figures 3a, 3c, 3e) we study the effect of amr. In the right column (Figures 3b, 3d, 3f) we study the effect of be, keeping fixed w.

(a) $\overline{\mathcal{U}}_1^{12}$ (b) $\overline{\mathcal{U}}_3^{12}$ (c) $\overline{\mathcal{U}}_4^{12}$
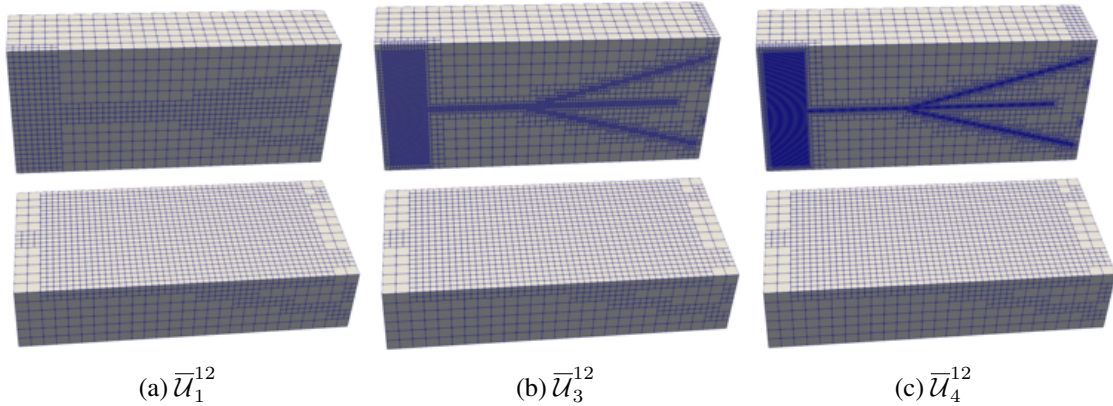
Figure 4: Sequences of meshes generated by iterating the AMR strategy.

4.2 Small Features

This benchmark example has been presented in [16] with the objective of probing the accuracy of discretization methods in the presence of small geometric features. The domain Ω is a box with dimensions $L_1 = L_3 = 1\,[\mathrm{m}]$ and $L_2 = 2.25\,[\mathrm{m}]$ and embeds a network of eight fractures. The geometrical setup and the material properties are the ones presented in [16].

Due to the high geometrical complexity of the fracture network, meshes for equi-dimensional formulations, which resolve the interfaces between the background and embedded fractures, are difficult to be generated. The AMR strategy at the base of the proposed approach enables a fully automatic generation of meshes for domains that contain a large number of highly complex heterogeneities. In Figure 4, we show some of the meshes generated by iterating several times the AMR strategy. Here, the superscript be refers to the number of subdivisions along the x_1-direction.
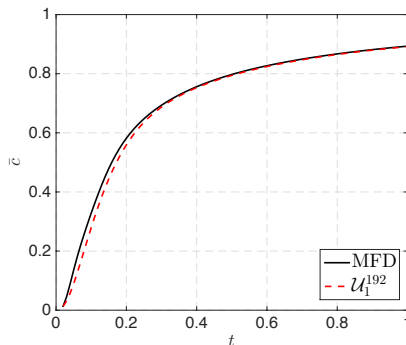
Figure 5: Comparison of the time evolution of mean concentration within one of the fracture (see [13] for more details) between the test case $\mathcal{U}_1^{192}$ and reference solution [13].

For the transport problem Γ_{in} coincides with the central strip on the left side of the domain,

on which we impose $g = 1.0$ [m^{-3}]. We refer to [16, 13] for more details. The rest of the boundary is Γ_{out}. We set $T_{\text{fin}} = 1.0$ [s] and $\Delta t = 0.01$ [s].

In Figure 5 we report the mean concentration computed over the simulation time in one the fracture and defined as $\frac{\int_{\Omega_F} c}{|\Omega_F|}$, where c is the concentration in fracture Ω_F and $|\Omega_F|$ is the corresponding volume. In particular, we choose the same fracture as in the benchmark paper [13]. A good agreement is found between the numerical solution computed on the mesh $\overline{\mathcal{U}}_1^{192}$ and the reference solution reported in [13].

In Figure 6, we show the distribution of the concentration at the time instants $t_1 = 0.0$ [s], $t_2 = 0.5$ [s] , and $t = T = 1.0$ [s] on the mesh $\overline{\mathcal{U}}_1^{192}$. The concentrations are always comprised between 0 and 1 for the entire simulated time, demonstrating the ability of the AFC scheme to ensure the DMP and to preserve the positivity of the solution.
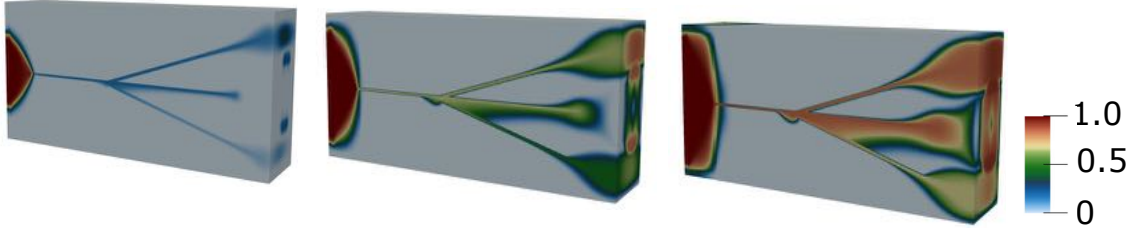
Figure 6: Concentration distribution at time $t_1 = 0.0$ [s], $t_2 = 0.5$ [s] , and $t = T = 1.0$ [s] for the test case $\mathcal{U}_1^{192}$.

5   Conclusion

We have presented a simulation framework for transport problems in fractured porous media based on an equi-dimensional model and a continuous FE method. These problems are particularly complicated to simulate due to the complex geometry of the fracture networks, and the large discontinuities in the material properties, The former one introduces difficulties in the mesh generation, while the latter one is responsible of introducing singularities in the solution, which reduce the accuracy of standard discretization methods.

The proposed framework presents some inherent advantages: i) it can be straightforwardly implemented in any standard FE library as, differently from the hybrid-dimensional models, ii) it does not involve the coupling of models with different dimensionalities; iii) it is element-wise conservative. Moreover, it provides an instrument to validate the commonly-used reduced hybrid-dimensional models, in particular on complex geometries for which the generation of suitable meshes is not feasible.

REFERENCES

[1] Susanna Gebauer, Lina Neunhäuserer, Ralf Kornhuber, Steffen Ochs, Reinhard Hinkelmann, and Rainer Helmig. Equidimensional modelling of flow and transport processes in fractured porous systems i. In *Developments in Water Science*, volume 47, pages 335–342. Elsevier, 2002.

[2] Lina Neunhäuserer, Susanna Gebauer, Steffen Ochs, Reinhard Hinkelmann, Ralf Kornhuber, and Rainer Helmig. Equidimensional modelling of flow and transport processes in fractured porous systems ii. In *Developments in Water Science*, volume 47, pages 343–350. Elsevier, 2002.

[3] Paola F Antonietti, Luca Formaggia, Anna Scotti, Marco Verani, and Nicola Verzott. Mimetic finite difference approximation of flows in fractured porous media. *ESAIM: Mathematical Modelling and Numerical Analysis*, 50(3):809–832, 2016.

[4] Inga Berre, Florian Doster, and Eirik Keilegavlen. Flow in fractured porous media: A review of conceptual models and discretization approaches. *Transport in Porous Media*, 130(1):215–236, 2019.

[5] Martin Petzoldt. Regularity results for laplace interface problems in two dimensions. *Zeitschrift für Analysis und ihre Anwendungen*, 20(2):431–455, 2001.

[6] Ridgway Scott. Finite element convergence for singular data. *Numerische Mathematik*, 21(4):317–327, 1973.

[7] Dmitri Kuzmin. Algebraic flux correction i. In *Flux-corrected transport*, pages 145–192. Springer, 2012.

[8] Thomas JR Hughes. A multidimentional upwind scheme with no crosswind diffusion. *Finite Element Methods for Convection Dominated Flows, AMD 34*, 1979.

[9] Franco Brezzi, Leopoldo P Franca, and Alessandro Russo. Further considerations on residual-free bubbles for advective-diffusive equations. *Computer Methods in Applied Mechanics and Engineering*, 166(1-2):25–33, 1998.

[10] Jesús Bonilla and Santiago Badia. Monotonicity-preserving finite element schemes with adaptive mesh refinement for hyperbolic problems. *Journal of Computational Physics*, page 109522, 2020.

[11] Marco Favino, Jürg Hunziker, Eva Caspari, Beatriz Quintal, Klaus Holliger, and Rolf Krause. Fully-automated adaptive mesh refinement for media embedding complex heterogeneities: application to poroelastic fluid pressure diffusion. *Computational Geosciences*, pages 1–20, 2019.

[12] M. Favino and M. G. C. Nestola. An equi-dimensional finite element approach for flow problems in fractured porous media. *WCCM-ECCOMAS2020*.

[13] Inga Berre, Wietse M Boon, Bernd Flemisch, Alessio Fumagalli, Dennis Gläser, Eirik Keilegavlen, Anna Scotti, Ivar Stefansson, Alexandru Tatomir, Konstantin Brenner, et al. Verification benchmarks for single-phase flow in three-dimensional fractured porous media. *Advances in Water Resources*, 147:103759, 2021.

[14] Richard S Varga. On a discrete maximum principle. *SIAM Journal on Numerical Analysis*, 3(2):355–359, 1966.

[15] Sergei K Godunov and I Bohachevsky. Finite difference method for numerical computation of discontinuous solutions of the equations of fluid dynamics. *Matematičeskij sbornik*, 47(3):271–306, 1959.

[16] Inga Berre, Wietse Boon, Bernd Flemisch, Alessio Fumagalli, Dennis Gläser, Eirik Keilegavlen, Anna Scotti, Ivar Stefansson, and Alexandru Tatomir. Call for participation: Verification benchmarks for single-phase flow in three-dimensional fractured porous media. *arXiv preprint arXiv:1809.06926*, 2018.

[17] Lars H Odsæter, Trond Kvamsdal, and Mats G Larson. A simple embedded discrete fracture–matrix model for a coupled flow and transport problem in porous media. *Computer Methods in Applied Mechanics and Engineering*, 343:572–601, 2019.

[18] Jürg Hunziker, Marco Favino, Eva Caspari, Beatriz Quintal, J Germán Rubino, Rolf Krause, and Klaus Holliger. Seismic attenuation in realistic fracture networks. In *Poromechanics VI*, pages 1565–1572. Sixth Biot Conference on Poromechanics, 2017.

[19] Jürg Hunziker, Marco Favino, Eva Caspari, Beatriz Quintal, J Germán Rubino, Rolf Krause, and Klaus Holliger. Seismic attenuation and stiffness modulus dispersion in porous rocks containing stochastic fracture networks. *Journal of Geophysical Research: Solid Earth*, 123(1):125–143, 2018.